INSTABILITY ANALYSIS OF THE FIBRE-MATRIX DEBOND ONSET AND GROWTH UNDER TRANSVERSE TENSION

L. Távara*[1], V. Mantič[1], E. Graciani[1]

[1] *Grupo de Elasticidad y Resistencia de Materiales, Departamento de Mecánica de Medios Continuos y Teoría de Estrucuturas, Universidad de Sevilla, Camino de los Descubrimientos s/n 41092, Sevilla, Spain*

* *Corresponding Author: ltavara@etsi.us.es*

Keywords: Fibre-matrix interface, debond, snap-back instability, BEM,

Abstract

The instability behaviour associated to a crack onset and propagation along the fibre-matrix interface in a composite system under remote transverse loads is studied by a means of the linear elastic - (perfectly) brittle interface model (LEBIM). LEBIM has proved to model adequately the behaviour of this interface represented by a continuous distribution of springs which simulates the presence of a thin elastic layer. The failure mechanism in the case of an isolated fibre under transverse tension (plane strain problem), i.e. the onset and growth of the fibre-matrix interface crack, is studied. The numerical results provided by a 2D boundary element analysis show that a fibre-matrix interface failure initiates by onset of a finite debond in the neighbourhood of an interface point where the failure criterion is reached first (under increasing proportional load), this debond further propagates along the interface in mixed mode or even, in some configurations, with the crack tip under compression.

1. Introduction

Several previous works by the authors and coworkers [1, 2, 3] study experimentally, numerically and semi-analytically the inter–fibre failure of a unidirectional composite lamina under biaxial transverse loads. Numerical models of a single fibre embedded in a large matrix, based on Boundary Element Method (BEM) and interfacial fracture mechanics, are presented in [1, 4, 5]. BEM and Linear Elastic-Brittle Interface Model (LEBIM) are used to study and characterize the behavior of the fibre-matrix interface in [3, 6, 7].

The aim of the present work is to study in detail the instability issues that appear in the single fibre problem. An extensive review of the literature about the problem of an elastic circular inclusion embedded in an elastic matrix with or without a partial debond can be found in [7]. Details of the LEBIM implementation in a BEM code are also presented therein. Some fundamental results regarding the computation of the Energy Release Rate (ERR) in the LEBIM can be found in [8].

The present paper is organized as follows. First the LEBIM used is briefly described. Then, a plane strain problem of a circular inclusion, representing a long fibre under a remote biaxial

transversal loading, is introduced. BEM is applied to the numerical solution of the fibre-matrix interface crack onset and growth in this problem. Finally, a discussion of the instabilities produced in the problem is presented.

2. LEBIM

As shown in [3, 6, 7], the LEBIM can be used in microscale models to simulate the damage initiation and propagation at the fibre-matrix interface. The LEBI constitutive law and the interface failure criterion were developed in [3, 6, 7, 9]. The continuous spring distribution that models the elastic layer (interphase) along the fibre-matrix interface is governed by the following simple linear elastic - (perfectly) brittle law written at an interface point x:

$$\begin{array}{ll} \text{Linear Elastic} & \left\{ \begin{array}{ll} \sigma(x) = k_n \delta_n(x) \\ \tau(x) = k_t \delta_t(x) \end{array} \right. \quad t(x) < t_c(\psi_\sigma(x)) \\ \text{interface} & \end{array}$$

$$\begin{array}{ll} \text{Broken} & \left\{ \begin{array}{l} \sigma(x) = \left\langle \begin{array}{ll} 0 & \delta_n(x) > 0 \\ k_n \delta_n(x) & \delta_n(x) \leq 0 \end{array} \right. \\ \tau(x) = 0 \end{array} \right. \\ \text{interface} & \end{array} \tag{1}$$

where $\sigma(x)$ and $\tau(x)$ are, respectively, the normal and tangential components of the tractions along the interface in the elastic layer, $\delta_n(x)$ and $\delta_t(x)$ are, respectively, the normal and tangential relative displacements between opposite interface points. k_n and k_t denote the normal and tangential stiffnesses of the spring distribution. The traction modulus t is defined as $t(x) = \sqrt{\sigma^2(x) + \tau^2(x)}$.

It should be noticed that the critical traction modulus $t_c(\psi_\sigma(x))$ is a function of a fracture mode mixity angle, ψ_σ, at an interface point x. This angle is defined by $\tan \psi_\sigma(x) = \tau(x)/\sigma(x)$. This fact leads to, in general, different values of the critical traction modulus at different interface points. Although the criterion is written in terms of tractions, $t(x) \leq t_c(\psi_\sigma(x))$, it is actually based on an energetic criterion. An extensive explanation of the deduction of the model can be found in [3, 6, 7, 9].

3. Problem of a circular inclusion under transverse loads

The plane strain problem of a circular inclusion of radius $a > 0$ embedded in an infinite matrix, initially without any debond along its interface, and subjected to remote uniform stresses is considered. The materials of both the inclusion and matrix are considered to be linear elastic isotropic. Let (x, y) and (r, θ) be the cartesian and polar coordinates with the origin of coordinates in the center of the inclusion, assuming without any loss of generality that (x, y) is the principal coordinate system of the remote stress state defined by the principal stresses $\sigma_x^\infty \geq \sigma_y^\infty$, see Fig. 1.

In the present work, which covers also configurations where both remote principal stresses are

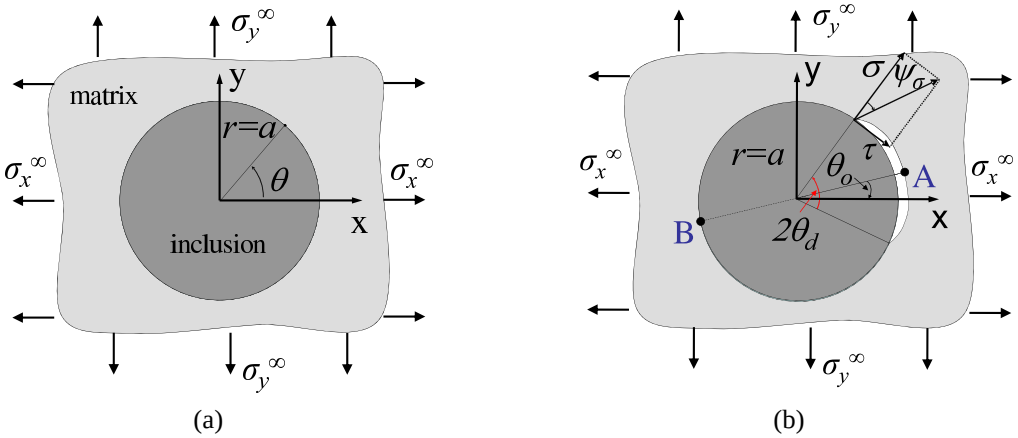

Figure 1. Inclusion problem configuration under biaxial remote transverse tension (a) without and (b) with a partial debond.

compressive, the following general *load-biaxiality parameter*[1]:

$$\chi = \frac{\sigma_x^\infty + \sigma_y^\infty}{2\max\{|\sigma_x^\infty|, |\sigma_y^\infty|\}}, \qquad -1 \le \chi \le 1, \tag{2}$$

is used. Denoting the Frobenius norm of the remote stress state by $S^\infty = \sqrt{(\sigma_x^\infty)^2 + (\sigma_y^\infty)^2}$, we have $\sigma_x^\infty = S^\infty \cos\phi^\infty$ and $\sigma_y^\infty = S^\infty \sin\phi^\infty$.

Let the position where the interface crack onset occurs be defined by the polar angle $\theta_o \in \langle 0°, 90°\rangle$. The semidebond angle is denoted as θ_d. During the debond growth the angle θ_o may or may not be placed at the center of the debond.

According to Fig. 1(b) only one debond, initiated at a point A($r = a$, $\theta = \theta_o$), is considered, although depending on the problem symmetry two or four equivalent positions for debond onset may exist at the inclusion interface with $\theta = \pm\theta_o, \pm\theta_o + 180°$. Nevertheless, according to the experimental evidence only one side of the fibre-matrix interface is usually broken [10, 11]. This will also be obtained by the present numerical model, where the crack onset can occur at any of these two or four points, but once a crack has started at one of these points it will continue growing, preventing failure in the other symmetrically situated points.

A typical bimaterial system among fibre reinforced composite materials is chosen for this study: *m*-epoxy matrix and *i*-glass fibre (inclusion), the elastic properties of matrix and fibre being $E_m = 2.79$ GPa, $\nu_m = 0.33$, $E_i = 70.8$ GPa and $\nu_i = 0.22$, respectively.

The strength and fracture properties of the fibre-matrix interface, tensile strength $\bar{\sigma}_c = 90$ MPa and fracture energy in mode I $\bar{G}_{Ic} = 2$ Jm^{-2}, considered in the numerical procedure are in the range of values found in the literature [10, 12], and correspond to quite brittle behaviour [2, 13] making the hypothesis of the LEBIM to represent appropriately a possible real composite material behavior [7].

[1] It is easily to see that χ gives the position of the center of the normalized Mohr circumference and its characteristic values are $\chi = 1$ - equibiaxial tension, $\chi = 0.5$ - uniaxial tension, $\chi = 0$ - equibiaxial tension-compression (pure shear stress), $\chi = -0.5$ - uniaxial compression and $\chi = -1$ - equibiaxial compression). It is useful to realize that $\phi^\infty = \frac{\pi}{2}\left(\chi - \frac{1}{2}\right)$.

In the following numerical study the following LEBIM propierties are used: ξ=0.25, λ=0.25 (characterizing the fracture toughness sensitivity on the fracture mode mixity) and a circular inclusion radius a=7.5 μm.

4. BEM model and numerical results

The present non-linear problem of the crack onset and propagation along the fibre-matrix interface governed by the LEBIM is solved by means of the BEM, which is very suitable for solving this kind of problems where all nonlinearities are placed on the boundaries of the subdomains. Implementation details of the collocational 2D BEM code employed and an overall description of the solution algorithm can be found in [6, 7, 9, 14]. This algorithm uses an incremental formulation and a very efficient solution procedure, usually referred to as sequentially linear analysis, appropriate for the present non-linear problem. The present BEM model represents a cylindrical inclusion with a radius a =7.5 μm inside a relatively large square matrix with side 2ℓ = 1 mm. BEM mesh has 1472 continuous linear boundary elements: two uniform meshes of 720 elements discretizing both sides of the fibre-matrix interface (therefore, the polar angle of each element is 0.5°) and 32 elements for the external boundary of the matrix, where the remote stresses σ_x^∞ and σ_y^∞ are applied. Rigid body motions are removed by the Method F2 introduced in [15], see also [14]. The inclusion is considered initially as bonded to the matrix along its perimeter by means of a continuous distribution of springs governed by the LEBIM. The debond onset and propagation is modeled by progressively breaking springs between boundary element nodes placed at both sides of the interface. Thus, the numerical procedure used is driven by the interface crack length and is able to analyse both snap-through and snap-back instabilities of a crack growth.

In Fig. 2 the numerical results obtained for different values of the load biaxiality parameter $\chi = 0, 0.25, 0.5, 0.75$ and 1 are presented. Recall that $\chi = 0.5$ corresponds to the case of uniaxial tension in the x-direction ($\sigma_y^\infty = 0$).

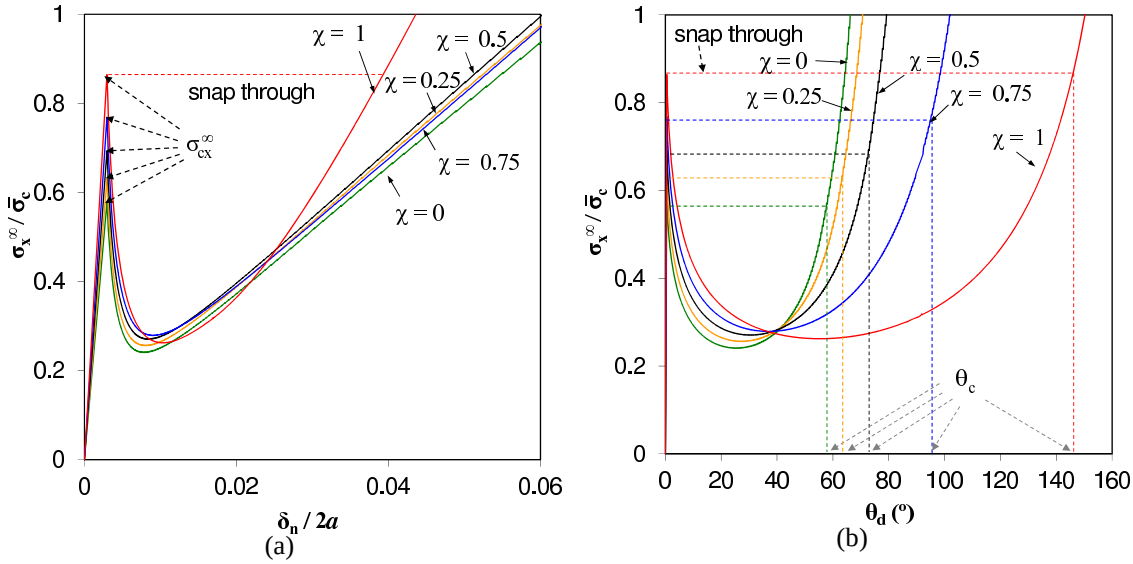

Figure 2. Numerical results. (a) The normalized applied stress with respect to the normal relative displacements δ_n at point A, see Fig. 1, and (b) The normalized applied stress with respect to the semidebond angle θ_d for different biaxial loads combinations, with ξ = 0.25 and λ=0.25.

In Fig. 2(a), the normalized remote stress $\sigma_x^\infty/\bar{\sigma}_c$ is plotted as a function of the normal relative displacement (opening), δ_n, evaluated at the point A($a, \theta_o = 0°$) defined in Fig. 1(b). The (minimum) remote stress value that is needed to initiate crack growth (in simple terms, the stress that is needed to break the first spring in the present discrete model of the interface) is called critical stress, σ_{cx}^∞, and corresponds to the local maximum of a function shown in Fig. 2(a). It can also be observed in Fig. 2(a) that after reaching the critical stress, σ_{cx}^∞, the crack growth becomes unstable, requiring smaller values of the remote tension to cause further crack growth. Thus, an instability phenomenon called snap-through is predicted in the case of remote load control, see Section 5.

5. Instability analysis

In the following section, the instability behaviour observed in Fig. 2 will be analysed under a remote load or displacement control. Although only the case of uniaxial tension ($\chi = 0.5$), with the default values of ξ and λ, is considered for the sake of brevity, the results would be similar for other values of the governing dimensionless parameters. Fig. 3(a) shows the normalized applied remote stress $\sigma_x^\infty/\bar{\sigma}_c$ versus the averaged longitudinal strain ε along the segments, AB and PQ, between two pairs of points of the matrix placed on the x-axis and symmetrically situated with respect to the origin. The coordinates of the end points of AB are ($x = \pm a, y = 0$) and of PQ ($x = \pm \ell, y = 0$), where a is the fibre radius and ℓ the half-length of the matrix square cell side, $\ell/a = 66.7$ in the present study. ε^e represents the averaged longitudinal strain for a purely linearly elastic fibre-matrix interface with no debond, while ε^d is the additional averaged longitudinal strain due to debond ($\varepsilon^d = \varepsilon - \varepsilon^e$). For a similar additive decomposition of relative displacements, see [16] (Ch. 12 therein).

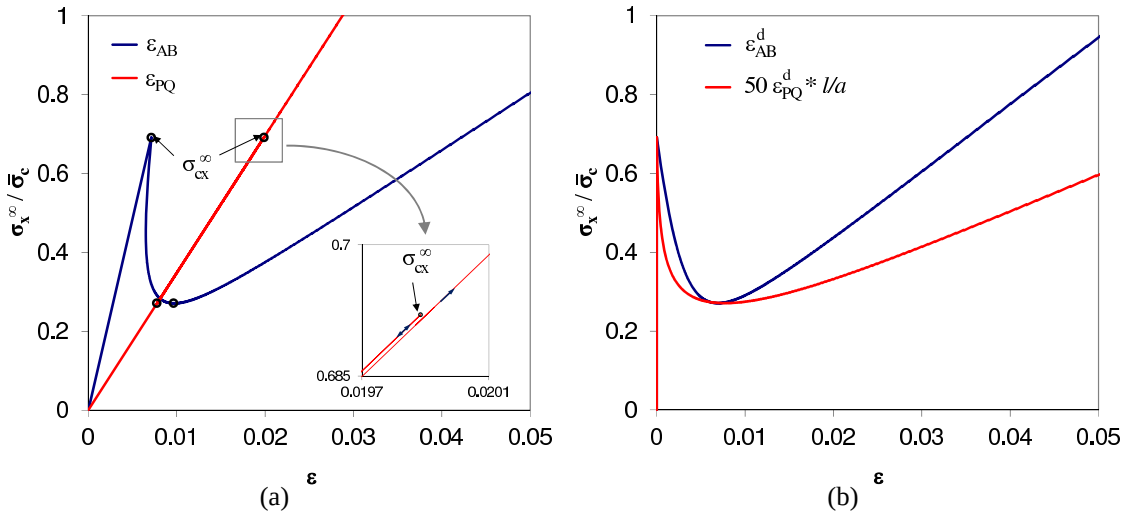

Figure 3. Numerical results. The normalized applied stress σ_x^∞ with respect to (a) the averaged longitudinal strains, $\varepsilon_{AB} = \varepsilon_{AB}^e + \varepsilon_{AB}^d$ and $\varepsilon_{PQ} = \varepsilon_{PQ}^e + \varepsilon_{PQ}^d$, and (b) the additional averaged longitudinal strain due to debond, ε_{AB}^d and the scaled one $50\frac{\ell}{a}\varepsilon_{PQ}^d$, with $\chi = 0.5$, $\xi = 0.25$ and λ=0.25.

The diagrams $\sigma_x^\infty - \varepsilon$ in both cases (considering segments AB and PQ) exhibit cusp snap-back instability [17] after the peak point (bifurcation point) where the debond onset occurs. Actually, this kind of instability also appears for all intermediate segments between AB and PQ. While the snap-back instability is easily observable in the curve $\sigma_x^\infty - \varepsilon_{AB}$ in Fig. 3(a), this instability

is not visible by naked-eye in the curve $\sigma_x^\infty - \varepsilon_{PQ}$, as the curve branches before and after the peak point are extremely close to each other, visually coinciding in the plot, because the matrix cell is very large with respect to the fibre. As the effect of the debond onset and growth on the fibre-matrix interface is hardly visible on this plot, a zoomed view of this curve with its cusp is also included in Fig. 3(a) to show this instability behaviour. Obviously the values of $\sigma_x^\infty/\overline{\sigma}_c$ at the local maxima (peak point) and minima in both curves coincide (values 0.692 and 0.2704, respectively) as indicated in the curve plots. It means that after the debond onset, we may decrease the applied load significantly, up to 39% of the critical load in the peak, keeping a continuous propagation of the debond.

Moreover, to understand better the post-peak behaviour, diagrams $\sigma_x^\infty - \varepsilon^d$ are plotted in Fig. 3(b). The value of ε_{PQ}^d, which strongly depends on the cell size ℓ (as a consequence of the Saint-Venant and superposition principles), is scaled by an arbitrary factor $50\,\frac{\ell}{a}$ resulting in a value very similar to that of ε_{AB}^d. The initial very steep negative slope of these diagrams indicates that according to the present model, using the LEBIM of the fibre-matrix interface, the debond onset and growth exhibits cusp snapback instability typical for a brittle structural behaviour. This observation is quite different from a smooth snapback instability observed in some cases in [18, 19] using a CZM of the fibre-matrix interface.

6. Conclusions

From the numerical results obtained, it can be observed that when the remote load reaches its critical value given by σ_{cx}^∞, the subsequent debond growth up to the critical semidebond angle θ_c is unstable, an instability phenomenon called snap-back and snap-through, respectively, taking place under remote displacement and load controls. A parametric study shows that θ_c increases with increasing χ in the range studied, eventually very large debonds with $\theta_c > 90^\circ$ are predicted when similar tensions are applied in both directions.

Summarizing the instability analysis, the curve $\sigma_x^\infty - \varepsilon_{PQ}$ shows that under both load and displacement control at the outer boundaries of the matrix cell a sudden and large breakage of the fibre-matrix interface is predicted by the present model. Notice that, the debond onset and growth could develop, at least hypothetically, in a stable manner if it would be controlled by the crack opening δ_n according to Fig. 2(a).

Acknowledgements

The work was supported by the Junta de Andalucía and the European Social Fund (Projects of Excellence TEP-1207, TEP-2045, TEP-4051, P12-TEP-1050), the Spanish Ministry of Education and Science (Projects TRA2006-08077 and MAT2009-14022) and Spanish Ministry of Economy and Competitiveness (Projects MAT2012-37387 and DPI2012-37187).

References

[1] F. París, E. Correa, and J. Cañas. Micromechanical view of failure of the matrix in fibrous composite materials. *Composites Science and Technology*, 63:1041–1052, 2003.

[2] V. Mantič and I.G. García. Crack onset and growth at the fibre-matrix interface under

remote biaxial transverse loads. Application of a coupled stress and energy criterion. *International Journal of Solids and Structures*, 49:2273–2290, 2012.

[3] V. Mantič, L. Távara, A. Blázquez, E. Graciani, and F. París. Application of a linear elastic-brittle interface model to the crack initiation and propagation at fibre-matrix interface under biaxial transverse loads. ArXiv preprint. arXiv:1311.4596, 2013.

[4] V. Mantič, A. Blázquez, E. Correa, and F. París. Analysis of interface cracks with contact in composites by 2D BEM. In M. Guagliano and M. H. Aliabadi, editors, *Fracture and Damage of Composites*, pages 189–248. WIT Press, Southampton, 2006.

[5] F. París, E. Correa, and V. Mantič. Kinking of transverse interface cracks between fiber and matrix. *Journal of Applied Mechanics*, 74:703–716, 2007.

[6] L. Távara. *Damage initiation and propagation in composite materials. Boundary element analysis using weak interface and cohesive zone models*. PhD Thesis. Universidad de Sevilla: Sevilla, 2010.

[7] L. Távara, V. Mantič, E. Graciani, and F. París. BEM analysis of crack onset and propagation along fiber-matrix interface under transverse tension using a linear elastic-brittle interface model. *Engineering Analysis with Boundary Elements*, 35:207–222, 2011.

[8] S. Lenci. Analysis of a crack at a weak interface. *International Journal of Fracture*, 108:275–290, 2001.

[9] L. Távara, V. Mantič, E. Graciani, J. Cañas, and F. París. Analysis of a crack in a thin adhesive layer between orthotropic materials. An application to composite interlaminar fracture toughness test. *Computer Modeling in Engineering and Sciences*, 58(3):247–270, 2010.

[10] H. Zhang, ML. Ericson, J. Varna, and LA. Berglund. Transverse single-fiber test for interfacial debonding in composites: 1. Experimental observations. *Composites Part A: Applied Science and Manufacturing*, 28A:309–315, 1997.

[11] E. Correa, E. K. Gamstedt, F. París, and V. Mantič. Effects of the presence of compression in transverse cyclic loading on fibre–matrix debonding in unidirectional composite plies. *Composites Part A: Applied Science and Manufacturing*, 38:2260–2269, 2007.

[12] J. Varna, LA. Berglund, and ML. Ericson. Transverse single fiber test for interfacial debonding in composites 2: Modelling. *Composites Part A: Applied Science and Manufacturing*, 28:317–326, 1997.

[13] V. Mantič. Interface crack onset at a circular cylindrical inclusion under a remote transverse tension. Application of a coupled stress and energy criterion. *International Journal of Solids and Structures*, 46:1287–1304, 2009.

[14] E. Graciani, V. Mantič, F. París, and A. Blázquez. Weak formulation of axi-symmetric frictionless contact problems with boundary elements: Application to interface cracks. *Computer and Structures*, 83:836–855, 2005.

[15] A. Blázquez, V. Mantič, F. París, and J. Cañas. On the removal of rigid body motions in the solution of elastostatic problems by direct BEM. *International Journal for Numerical Methods in Engineering*, 39:4021–4038, 1996.

[16] Z. Bažant and L. Cedolin. *Stability of Structures Elastic, Inelastic, Fracture and Damage Theories*. Oxford University Press: New York, 1991.

[17] A. Carpinteri. Cusp catastrophe interpretation of fracture instability. *Journal of the Mechanics and Physics of Solids*, 37:567–582, 1989.

[18] A. Carpinteri, M. Paggi, and G. Zavarise. Snap-back instability in micro-structured composites and its connection with superplasticity. *Strength, Fracture and Complexity*, 3:61–72, 2005.

[19] M. Paggi, I.G. García, and V. Mantič. Fiber-size effects on the onset of fiber-matrix debonding under transverse tension: A comparison between cohesive zone and finite fracture mechanics models. *Engineering Fracture Mechanics*, 115:96–110, 2014.